Spectrochimica Acta Part A: Molecular and Biomolecular Spectroscopy 352 (2026) 127561

Contents lists available at ScienceDirect

Spectrochimica Acta Part A:
Molecular and Biomolecular Spectroscopy

journal homepage: www.journals.elsevier.com/spectrochimica-acta-part-a-molecular-and-biomolecular-spectroscopy

Application of FTIR and PCA-LR metabolites recognition for bergamot essential oil authentication

Laura Manin [a,b], Giuseppe Oliva [a], Maria Giovanna Bianco [c], Md. Maruf Hossain [d], Srećko Valić [b,e], Syed K. Islam [d], Filippo Laganà [a], Antonino S. Fiorillo [a], Salvatore A. Pullano [a,d,*]

[a] Department of Health Sciences, University "Magna Græcia" of Catanzaro, 88100, Catanzaro, Italy
[b] Department of Medical Chemistry Biochemistry and Clinical Chemistry, University of Rijeka, 51000, Rijeka, Croatia
[c] Department of Medical and Surgical Sciences, University "Magna Græcia" of Catanzaro, 88100, Catanzaro, Italy
[d] Department of Electrical Engineering and Computer Science, University of Missouri, Columbia, MO 65211, USA
[e] Division of Physical Chemistry, Ruđer Bošković Institute, 10000, Zagreb, Croatia

HIGHLIGHTS

- FTIR spectroscopy combined with PCA-LR enables rapid and non-destructive BEO authentication.
- A multiclass classification model proficiently differentiates between natural, synthetic, and adulterated BEO samples with high accuracy.
- This approach strengthens quality control, helps prevent fraud, and paves the way for a device for rapid and accessible BEO analysis.

GRAPHICAL ABSTRACT

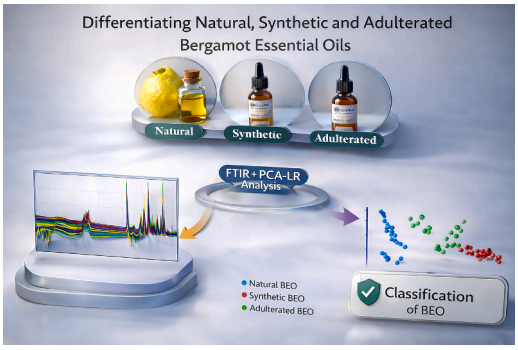

ARTICLE INFO

Keywords:
FTIR-ATR
Synthetic BEO
Adulterated oil
NMR
Chemometric classification

ABSTRACT

A rapid method using FTIR-ATR spectroscopy combined with PCA and a classification model was applied to distinguish between natural, synthetic, and adulterated Bergamot essential oil (BEO). Synthetic BEOs are often composed of specific alcohols such as ethanol and dipropylene glycol (DPG), which are used to dilute synthetic metabolites like limonene, linalyl acetate, and linalool. Synthetic BEOs exhibited a distinct peak at 1340 cm^{-1}, linked to C—H bending of alcohols or methyl group deformation in artificial esters like linalyl acetate, a peak that is absent in natural BEOs. Additionally, an absorption band between 3600 and 3100 cm^{-1} indicated the presence of DPG and synthetic ethanol, a byproduct of synthetic linalyl acetate. These findings were validated by comparison with NMR spectroscopy for metabolite recognition. A logistic regression (LR) model using PCA was applied to 369 samples, achieving an overall accuracy of 0.976 ± 0.016 through five-fold cross-validation (CV).

* Corresponding author at: Department of Health Sciences, University "Magna Græcia" of Catanzaro, 88100 Catanzaro, Italy.
E-mail address: pullano@unicz.it (S.A. Pullano).

https://doi.org/10.1016/j.saa.2026.127561
Received 14 November 2025; Received in revised form 16 January 2026; Accepted 4 February 2026
Available online 6 February 2026

1. Introduction

Nowadays, there is a high demand for natural essential oils due to their limited production. Synthetic oils, also known as fragrance oils, are artificially created aromatic compounds designed to imitate the scent of natural essential oils but with several differences. The addition of low-cost essential oils, such as lavender or lemon, and/or synthetic compounds like linalyl acetate or linalool, significantly affects the quality of high-value pure essential oils [1]. Synthetic mixtures of different compounds are often used as alternatives to natural essential oils. However, as they do not contain natural components, they cannot offer the same aromatherapeutic effects [1,2]. Another aspect related to the properties and quality of essential oils is adulteration. The rising demand for high-value essential oils seems to have intensified adulteration practices, as producers seek to cut costs and increase product availability [1–4]. Although adulteration reduces the quality of the oils, it often provides limited benefits and can have harmful effects on human health. Bergamot (*Citrus bergamia Risso*) is a high-demand product on the market [5]. The production of bergamot essential oil (BEO) is geographically limited to a specific area of Reggio Calabria in Italy, which accounts for more than 90% of the global production. BEO is obtained by cold pressing the exocarp of the fruit, consisting of a volatile part (~93%) and a non-volatile part (~7%). The three compounds most present in the volatile fraction are limonene (25–45%), linalyl acetate (21–41%) and linalool (3–22%) [6]. However, the non-volatile fraction contains furanocoumarins such as bergapten (5-methoxypsoralen), a phototoxic compound known to induce skin irritation upon exposure to ultraviolet (UV) light [7,8]. Consequently, furanocoumarins are removed to enhance safety, particularly in cosmetic formulations. Despite its phototoxic potential, bergapten itself has been reported to exhibit diverse pharmacological properties, including neuroprotective, anticancer, anti-inflammatory and antidiabetic activities [9,10]. Bergamot oil has various medical uses, including as an antidepressant, antibiotic, antipyretic, and for treating skin diseases like psoriasis. It supports cardiovascular and nervous system health, improving cognitive functions [11–13]. Naringin, a component of bergamot, enhances insulin sensitivity and glucose tolerance, benefiting diabetics [14]. Bergamot also contains flavonoids such as neoeriocitrin and neohesperidin with antioxidant properties [15]. Studies show it lowers total and LDL cholesterol in patients with hypercholesterolemia [16]. Additionally, bergamot oil is used as a natural preservative in cosmetics, offering benefits like anti-acne, anti-aging and skin lightening [17–20]. Since bergamot essential oil has characteristic fresh citrus scent, it is used as top notes in various perfumes, which consumers first detect. Therefore, it is not surprising that the perfume industry shows interest in the research of essential oils and their economically profitable production [20]. Recently, sophisticated adulterations of bergamot oil have appeared, which include the addition of characteristic molecules isolated from other natural sources, such as linalyl isolated from *Cinnamomum camphora* (Camphor tree) or *Salvia sclarea* (clary sage), α-terpineol isolated from limonene and linalool isolated from lavender. Furthermore, different commercially available synthetics have been added to bergamot oil to create artificial mixtures, whose main purpose is to recreate natural essential oils with minimal costs. Producers usually dilute the essential oil using a carrier oil, alcohol and other synthetic components [20–23]. To prevent adulteration of EOs, the ISO standard 9235:2021 has been defined for essential oils as a fragrant product obtained from various plant raw materials by steam distillation [22]. Detection of EOs adulteration usually implies the use of standard techniques such as gas chromatography (GC) or high-performance liquid chromatography (HPLC) and nuclear magnetic resonance (NMR) [24–30]. Before the GC and HPLC analysis, oil samples often need to undergo several preparation steps, such as extraction, filtration or derivatization, which can be time-consuming and complex [25–27]. NMR spectroscopy does not require special preparation, other than dissolving the sample in a deuterated solvent [30]. However, it is more sophisticated, and the equipment is more expensive compared to Fourier transform infrared (FTIR) spectroscopy [30,31]. FTIR also enables the analysis of biological samples and the identification of chemical composition. Analysis takes only a few minutes. Sample preparation is minimal, without the need for solvent extraction or chemical modification [31]. FTIR allows the identification of specific molecular structures like fatty acids and triglycerides in the "fingerprint region" (600–1500 cm^{-1}), making it easier to detect the presence of foreign or adulterating oils [32–34]. Recent studies have demonstrated the broad applicability of FTIR spectroscopy combined with multivariate analysis for the rapid characterisation and discrimination of complex chemical systems [35–38]. The aim of this study was to develop a FTIR–based technique combined with chemometric analysis to authenticate BEO samples. High-resolution NMR spectroscopy was employed as an independent reference technique to support the FTIR-based. To the best of our knowledge, this study provides the first insight into the metabolite composition of synthetic bergamot essential oil.

2. Materials and methods

2.1. Oil samples

In this study, two types of essential oils were analysed to investigate differences in chemical composition and oil quality. The natural BEO samples were supplied by Azienda Agricola Minnici (Bianco, Italy), and the essential oil was extracted from the exocarp of three *Citrus bergamia Risso* cultivars: Castagnaro, Femminello, and Fantastico. All the cultivars were grown in the same pedoclimatic conditions in the Calabria region. A total of 199 natural BEO samples were obtained directly after extraction and subjected to defurocoumarinization, a standard industrial process aimed at removing phototoxic linear furocoumarins. A total of 100 synthetic BEO samples were purchased from Lotus House (Thailand), a commercial supplier. These samples are representative of commonly used adulterants in the fragrance and flavour industries. A total of 369 BEO samples were included in the analysis, consisting of 199 natural, 100 synthetic, and 70 adulterated samples. Adulterated BEO samples were prepared by *v*olumetric mixing of natural and synthetic bergamot essential oils at defined concentrations ranging from 15% to 60% (*v*/v) of synthetic oil. All mixtures were homogenised by gentle stirring prior to analysis to ensure compositional uniformity. All samples were stored in amber glass vials at room temperature and protected from light to minimize oxidative degradation and preserve their volatile composition prior to analysis.

2.2. Sample preparation

FTIR-ATR spectra were acquired using a Thermo Scientific NICOLET 6700, equipped with a Smart iTR™ (i.e. germanium crystal). A volume of 0.5 μL of each oil sample was placed on the ATR crystal. Each spectrum consists of 50 co-added scans, with a total acquisition time of approximately 100 s and a spectral resolution of 4 cm^{-1}, covering the range of 4000–650 cm^{-1}. As already mentioned, FTIR-ATR analysis does not require any prior preparation of the oil sample [33,34]. For NMR, analysis 50 μL of each of the oil samples was mixed with 500 μL of deuterated chloroform ($CDCl_3$, 99.8 atom % D; Sigma-Aldrich/Merck) and placed in a 5 mm NMR tube. Tetramethylsilane (TMS, ≥99.9%, NMR grade; Sigma-Aldrich/Merck) was used as a referent signal for ^1H NMR spectra. ^1H and ^{13}C NMR spectra were recorded at room temperature using a Bruker Avance 600 equipped with a 14 T superconducting magnet. SpinWorks 4.2.11 software was used for processing complex spectra of BEO samples. The data from 1D NMR FIDs (Free Induction Decay) were processed by Fourier transformation, phase corrected, baseline corrected and aligned using the TMS signal as a reference [39–41].

2.3. Spectral signal processing

The BEO spectral signal acquisition and processing was performed as shown in Fig. 1. As most of the natural compounds are affected by significant variability, a preprocessing analysis was standardized and implemented to improve SNR of the spectra. FTIR spectra of essential oils characteristically contain peaks in the region of O—H stretching (3400–3650 cm^{-1}), C—H stretching (3020–2900 cm^{-1}), C═O stretching (~1730 cm^{-1}), C—C stretching of the aromatic ring (~1450 cm^{-1}) and C—O stretching (~1237–1240 cm^{-1}) from monoterpenes and sesquiterpenes present in essential oils. The stretching vibrations of cyclic monoterpenes are predominant in essential oils, which are observed at 1645 cm^{-1}, 1435 cm^{-1} and 760 cm^{-1}(fingerprint region), and the C═O stretching of aldehydes and esters at 1739 cm^{-1} [42,43]. Pre-processing of spectra was performed in two main steps. Noise reduction and drift were taken into consideration by spectrum preprocessing. Raw spectra were analysed in the range (4000–650 cm^{-1}) and in a specific part of fingerprint (1500–1100 cm^{-1}). Spectra were smoothed using the Savitzky–Golay method considering a 2nd order polynomial and a window length of 9 points. Baseline drift and the normalization of data were performed after a second derivative and the extended multiplicative scattering correction (EMSC) was applied on mean centred data. Unit vector normalization (UNV) was applied to standardize intensity variations and enhance the comparability of spectral features [44,45].

2.4. Multivariate data analysis

Multivariate data analysis enables the observation, exploitation, and processing of multiple statistical variables to extract relevant synthesized information through both unsupervised (e.g., PCA) and supervised (e.g., Logistic Regression) methods. Initially, PCA was applied to examine pattern variability and improve interpretability. The FTIR spectra were decomposed into principal components (PCs), representing linear combinations of the original variables, as $X = SLS + RX = SL^S + R$, where X represents the pre-processed oil spectra, S denotes the scores, L the loadings, and R the residuals. Here, S is used to evaluate clustering patterns among samples, L identifies the variables with the greatest impact on score patterns, and R highlights any potential errors. Thus, PCA was employed for data dimension reduction, feature extraction, and finally for the most important pattern recognition [46]. This step aims to remove redundant or correlated features and retain only the most significant components, which capture most of the data variance. By reducing the number of input dimensions, PCA helps to improve computational efficiency and potentially reduces overfitting in the classifier models. This is followed by the application of logistic regression to the PCA scores to perform classification. This combination is particularly advantageous in chemometrics because logistic regression, with its clear probabilistic interpretation, handles multivariate data effectively and enables straightforward discrimination between classes. The efficacy of LR in classifying biological species was recently demonstrated using near-infrared spectroscopy, showcasing its robustness, interpretability, and ability to model linear relationships between features and the logit of probability in chemometric analyses [47]. The framework was implemented in Python 3.9 and scikit-learn 1.0.1. In this study, we employed a stratified k-fold cross-validation approach to ensure robust evaluation across all classes (a 5-fold cross-validation, repeated for 5 times). Multiclass performance was assessed using macro, micro, and weighted metrics (accuracy, precision, recall, and F1-score), providing insights into the behaviour of the model across datasets. ROC-AUC was calculated for each class in a one-vs-rest scheme to evaluate discrimination capabilities [48].

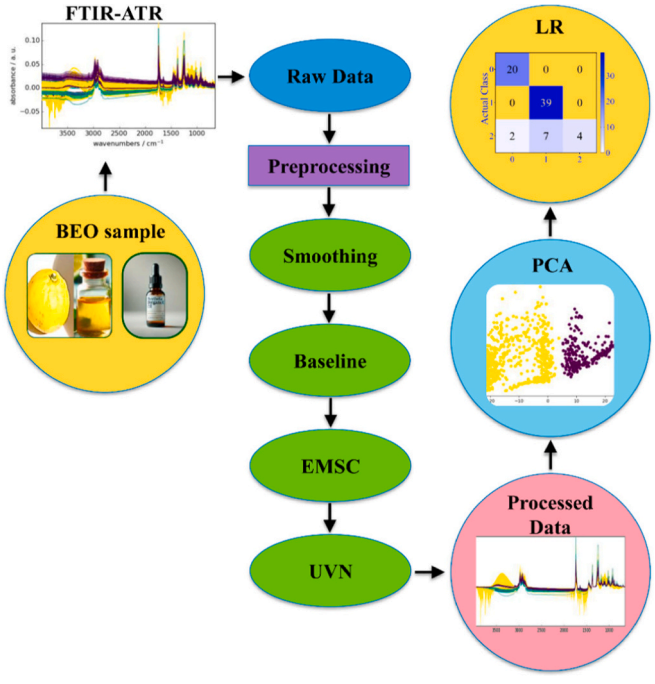

Fig. 1. Schematization of the experimental design including BEO sampling, spectral acquisition. Preprocessing, and classification.

3. Results and discussion

3.1. FTIR-ATR of natural and synthetic BEO

Natural bergamot essential oil is primarily composed of volatile unsaturated hydrocarbons with a pleasant smell such as monoterpenes, sesquiterpenes and oxygenated components [45]. The production of natural BEO, which forms the basis of almost all perfume essences, is limited both due to agro-climatic factors and due to the costs of the production itself. This has resulted in the growth of artificial mixtures in the market [23,49]. Notably, more than 90% of global natural BEO production is concentrated in the Reggio Calabria province (Italy); therefore, focusing on samples from this area is unlikely to limit the generalisability of the present study [50]. Several FTIR pre-processing alternatives are available [33,44]. In this study, the final workflow reported in Fig. 1 was selected after optimization to maximize signal-to-noise ratio and minimize baseline/scatter-related variability while preserving discriminative spectral information [42,44]. A representative FTIR-ATR spectrum of natural bergamot oil is reported in Fig. 2a. Characteristic stretching vibrations of the O—H group (~3400–3650 cm^{-1}), C═O stretching of the aldehydes (~1739 cm^{-1}), C—C stretching in the aromatic ring (~ 1452 cm^{-1}) and stretching of the acetate (esters) (~1237–1240 cm^{-1}) can be observed. The O—H stretching mainly comes from monoterpene and sesquiterpene alcohols present in natural bergamot essential oil.

In addition, from the same spectrum, it is possible to determine the composition of fatty acids present in the oil. As evidenced, fthe band at 3000 cm^{-1} represents C—H stretching within phospholipid molecules, which indicates the presence of fatty acids of different degrees of unsaturation. Moreover, the band at 1458 cm^{-1} results from the CH_2 bending vibration inside the molecules of unsaturated fatty acids which are proven to appertain from oleic and linoleic fatty acids [51,52]. The main FTIR adsorption bands and the specific components of natural bergamot oil are summarized in Table 1.

A representative FTIR-ATR spectrum of synthetic BEO is shown in Fig. 2b. Synthetic BEOs are obtained by blending a limited number of compounds to mimic BEO characteristics, so it is plausible that products from different manufacturers share similar profiles, reducing concerns about generalizability. Clear differences in chemical composition are visible in comparison with the natural essential oil of bergamot as shown in Fig. 2a. The main differences are observed in the intensity of

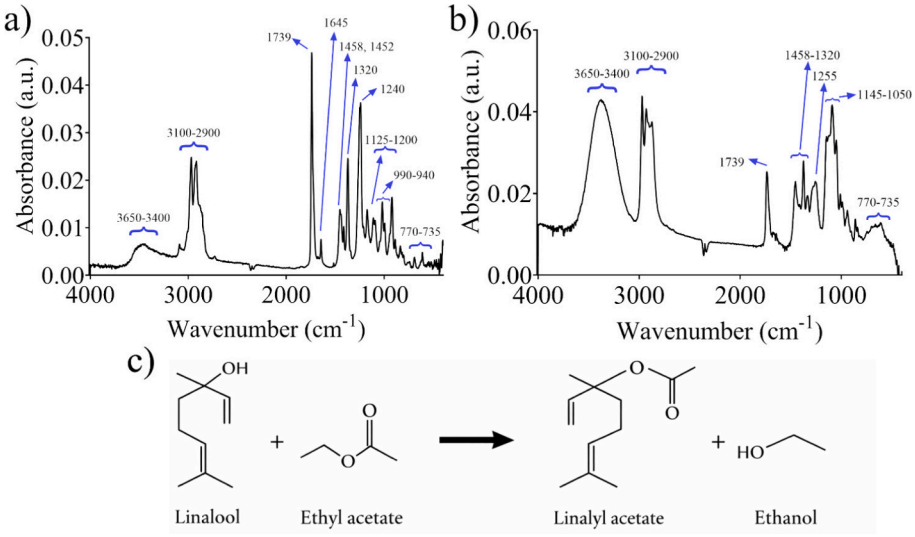

Fig. 2. (a) FTIR-ATR spectrum of natural bergamot essential oil (raw data) and (b) synthetic bergamot essential oil (raw data) (c) Synthesis of linalyl acetate.

Table 1
Characteristic IR bands present in natural BEO.

Wavenumber (cm^{-1})	Functional groups	Main components	Ref.
3650–3400	O-H stretch	Octanol, Linalool, Terpinen-4-ol, α- terpineol, Nerol, Citronellol, Geraniol, (*E*)-nerolidol, Campherenol, α -bisabolol	[53]
		Alkenes	[54]
3020–2900	H-C=C-H stretch	Unsaturation index of phospholipid acyl chains	[55]
1739	C=O stretch in aldehydes	Nonanal, Decanal, Neral, Geranial, Citronellal, Undecanal, Tetradecanal	[53]
	C=O stretch in ester groups in triacylglycerols	Unsaturated fatty acids	[55]
1645	C=C symmetrical stretch	Myrcene, Ocimene	[53,56]
1458	CH_2 bending vibration of lipids (fatty acids)	Oleic acid, Linoleic acid	[55]
1452	C-C stretches in the aromatic ring	α-, β- pinene, α-phellandrene, α- terpinene, p-cymene, γ-terpinene, Terpinolene, Limonene	[37,53]
1320	C-O stretch	Alcohols, Esters	[57]
1240	Acetate stretch	Linalyl acetate, Neryl acetate, Hexyl acetate, Heptyl acetate, Octyl acetate, Bornyl acetate, Nonyl acetate, α- Terpinyl acetate, Citronellyl acetate, Geranyl acetate, Decyl acetate	[53,57]
1200–1125	C-O stretch, tertiary alcohol	Linalool, Terpinen-4-ol	[53,58]
1000–650	=C–H bend	Alkenes	[54]
990–940	Trans RCH=CHR	C=C trans bending (out of plane)	[59]
770–735	Aromatic C—H out-of-plane bending	Aromatic compounds	[38,53]

absorption in the region of O—H stretching (~3400–3650 cm^{-1}) and in the band absorption observed at 1739 cm^{-1} from C═O stretching within the aldehyde. Moreover, in the fingerprint region (1500–600 cm^{-1}), differences in the peak at 1452 cm^{-1} which represents the stretching of the C—C bond within the aromatic ring and in the region of acetate stretching (~1237–1240 cm^{-1}) are observed. Natural BEO is rich in aromatic compounds, the most abundant of which is the already mentioned to be limonene. According to its chemical structure, limonene is a cyclic monoterpene which, as reported by Yahaya et al., absorbs IR radiation and gives peaks at 1645 cm^{-1}, 1435 cm^{-1}, and 760 cm^{-1} [60]. According to Fig. 2a, and b, the peak at 1452 cm^{-1} and peaks in the region of 770–735 cm^{-1} indicate the presence of limonene. Comparing the peaks of limonene reported by Yahaya et al. and the obtained peaks, a shift in wave numbers is visible [60]. The reason for such a shift can be attributed to the deformation of the aromatic ring and to the intermolecular bonds that limonene achieves with other molecules present in the oil. The abovementioned deformation of aromatic ring is one of characteristics of natural bergamot essential oil [61]. Other characteristic peak detected at 1240 cm^{-1} represents C—O ester stretching assigned to linalyl acetate [62]. Key differences between the synthetic and the natural bergamot essential oil were detected in the stretching region of the O—H group (~3400–3650 cm^{-1}) and in the fingerprint area, in the C—C stretching region within the aromatic ring (~1452 cm^{-1}) and in the C—O ester stretching region (~1237–1240 cm^{-1}). Stretching of the O—H group is attributable to synthetic bergamot oil, which indicates the use of alcohols and carrier oils [23,62–65]. The most used alcohol is DPG, whose IR spectrum shows similarities with the spectrum of synthetic BEO. The main function of used DPG is to assign the fragrance by the process of evaporation and at the same time dilute the essential oils, which are often expensive [23,64,65]. Despite the presence of DPG, the results indicate that artificial linalool was added to synthetic bergamot oil. As is known, the synthesis of linalool includes *β*-pinene involved in several consecutive steps. First, *β*-pinene is hydrogenated to pinane using a Pd/C catalyst. Next, pinane is oxidized to pinane-hydroperoxide with molecular oxygen. The resulting pinane-hydroperoxide is then subjected to hydrogenation over a Pd/C catalyst to yield pinanol. Finally, pinanol undergoes thermal isomerization to form linalool. Linalool represents the key compound for synthesis of geraniol, nerol and cytral that are also present in the natural BEO [64–66]. In addition to alcohols, carrier oil is also added, which is produced by pressing sweet almond, peach, apricot pit, sunflower seeds, sesame and jojoba [23,65]. These carrier oils are added to increase the oxidation stability of the essence, and given that they have no scent, they are excellent for dilution. The peak at 1452 cm^{-1} is attributed to the C—C stretching of limonene and *β*-pinene, as can be seen in Fig. 2a and b, there is a noticeable difference in absorption intensity. Absorption intensity of C—C stretch is higher in natural essential oil, which indicates the deficiency of limonene and *α*-pinene in the

synthetic bergamot oil. The lack of β-pinene suggests its use for the synthesis of linalool [64–66]. Limonene is responsible for the citrusy scent that represents the top notes of the essence, while β-pinene has the woody resinous scent that makes up the bottom notes [63]. C—O stretching of esters in bergamot oil is attributed to acetates, among which linalyl acetate is the most abundant. Linalyl acetate has a floral lavender scent that represents the heart notes of the essence [23,64,66]. From the obtained results, it can be observed that the peaks in the region of C—O stretching (~1237–1240 cm^{-1}) in synthetic BEO are of greater intensity, which indicates the addition of synthetically derived linalyl acetate. Linalyl acetate is most often produced by transesterification from linalool, a tertiary monoterpene alcohol and ethyl acetate (see Fig. 2c) [67].

3.2. PCA-LR prediction model

In Fig. 3a is shown the full spectra (4000–650 cm^{-1}) of 300 natural and synthetic BEO samples. The highlighted green region (3600–3100 cm^{-1}) emphasizes the O—H stretching vibration, a characteristic feature of synthetic oil containing DPG and ethanol, byproducts of the synthetic linalyl acetate synthesis. In contrast, Fig. 3b presents both spectra in the region of 1500 cm^{-1} to 1100 cm^{-1}. Notably, in this region, the FTIR

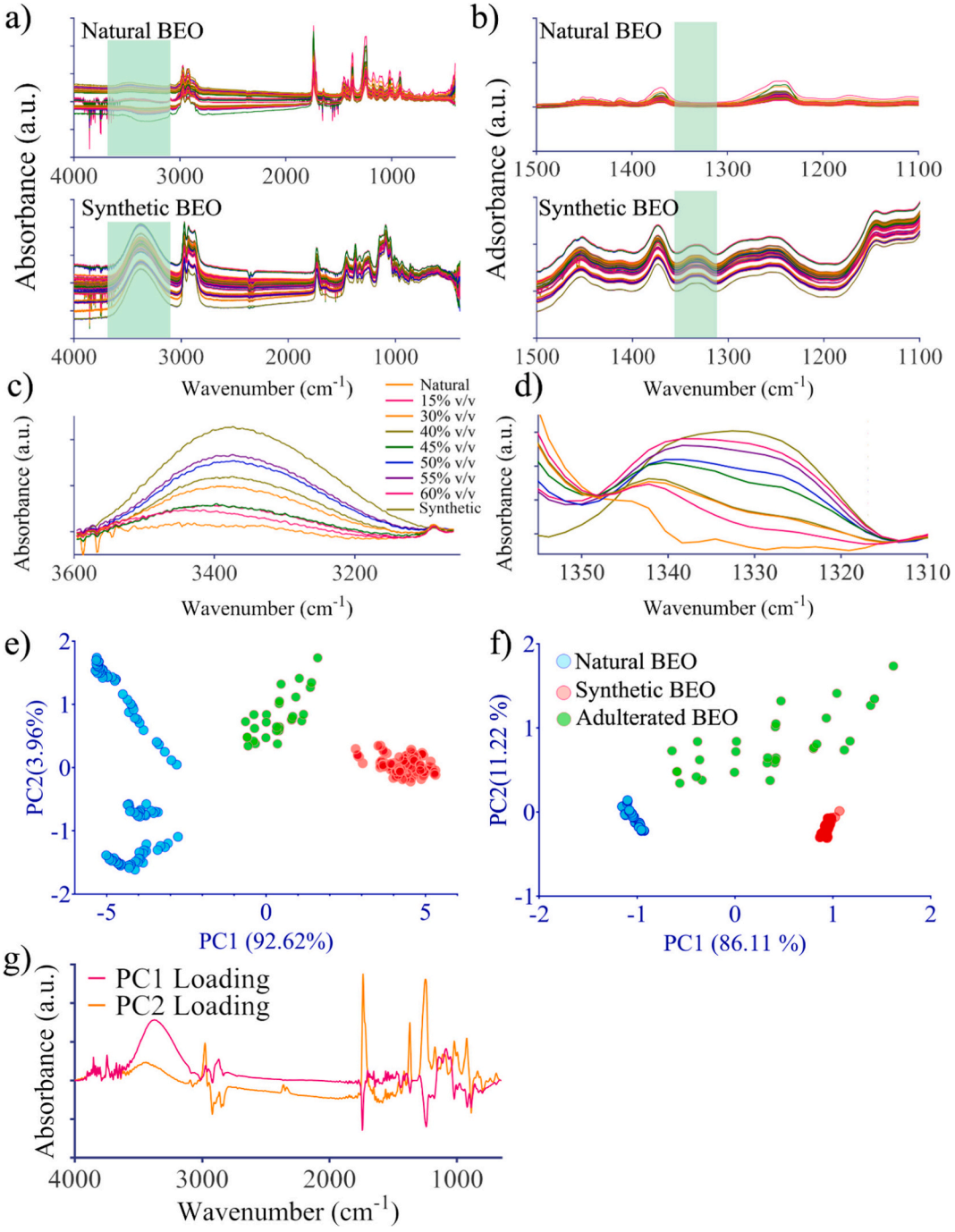

Fig. 3. (a) FTIR-ATR spectra of natural and synthetic BEO in the range of 4000 cm^{-1} to 650 cm^{-1}. (b) spectra of natural and synthetic BEO in the range of 1500 cm^{-1} to 1100 cm^{-1}. (c) spectra of BEO samples with varying degrees of adulteration in the range of 3600–3100 cm^{-1}. (d) spectra of BEO samples with varying degrees of adulteration in the range of 1355–1310 cm^{-1}. (e) PCA score plot of natural, synthetic and adulterated BEO based on full spectra (4000–650 cm^{-1}), and (f) on spectra within the range from 1500 to 1110 cm^{-1}. (g) principal component loadings (PC1 and PC2) obtained from full spectra PCA analysis.

spectrum of synthetic BEO shows a distinct peak at 1340 cm^{-1}, which is absent in the spectrum of natural BEO. This peak at 1340 cm^{-1} typically corresponds to C—H bending *v*ibrations present in alcohols (ethanol, DPG) or symmetric deformation of methyl (CH_3) groups often associated with synthetic compounds, such as artificial esters like linalyl acetate, which may not be present in natural BEO [68,69].

To emphasize potential variations in chemical composition resulting from dilution, adulteration with other essential oils, 70 spectra of mixtures containing natural and synthetic BEO at different concentrations were compared to those of the natural BEO. In Fig. 3c, an increasing absorption intensity of the O—H band (3600–3100 cm^{-1}) can be observed as the level of adulteration of BEO increases, starting from samples containing 15% to 60% *v*/v of synthetic BEO, respectively. Similarly, the same pattern of behaviour in adulterated BEO was observed in the region of C—H bending vibrations (1355–1310 cm^{-1}) (see Fig. 3d). PCA analysis was performed on 370 BEO samples (150 natural BEO, 150 synthetic BEO, and 70 mixed BEO), on the whole spectra and in the range from 1500 to 1110 cm^{-1} (see Fig. 3e and f). PCA analysis revealed three distinct clusters, indicating a notable transition of BEO samples based on their authenticity and different degrees of adulteration. To further identify the wavenumbers contributing most significantly to the differentiation between natural, synthetic, and adulterated BEO samples, PCA loading plots were analysed (see Fig. 3g). The PC1 loading plot revealed prominent peaks at approximately 3600–3100 cm^{-1}, 1732 cm^{-1}, 1340 cm^{-1} and 1240 cm^{-1} suggesting that these spectral regions are the key discriminators in class separation. The region 3600–3100 cm^{-1} corresponds to O—H stretching, likely from ethanol and dipropylene glycol (DPG). The 1732 cm^{-1} region reflects C═O stretching, indicative of ester functionalities (e.g., linalyl acetate), while the 1340 cm^{-1} band supports the presence of CH_3 bending vibrations linked to synthetic additives, including dipropylene glycol (DPG), commonly used as a solvent in synthetic BEO formulations. The additional band at 1240 cm^{-1} corresponds to C—O stretching of esters, further confirming the presence of acetate groups from linalyl acetate.

A stratified cross-validation procedure was employed to ensure a robust evaluation of the classification model using three classes (natural, synthetic, and adulterated BEO). In this case, a 5-fold stratified cross-validation was implemented, meaning the dataset was split into five subsets, and the model was trained and validated iteratively on these subsets to minimize overfitting and assess its generalization performance. A Logistic Regression model was then applied with a fixed random seed to ensure reproducibility. We ensured a leakage-safe evaluation procedure, class labels were handled strictly as the target variable and were never included among the input features (e.g., when using PCA score tables, only the PC scores were used as predictors, while the class column was excluded from the feature matrix). Predictions were made on the test subset, including class labels and class probabilities for all three classes. Out-of-fold predictions were used to compute performance metrics, ensuring that each sample was evaluated by a model that had not been trained on it. The Receiver Operating Characteristic (ROC) curve for each class was generated using the predicted probabilities, and the Area Under the Curve (AUC) was computed to quantify the discrimination power of the model. The ROC curves were interpolated to allow for the calculation of an average curve across folds. Moreover, accuracy, sensitivity and specificity were calculated for each fold. After completing the cross-validation, the classification performances were averaged to provide a summary of the overall performance of the model. The average ROC curve and the confusion matrix for Logistic Regression model are shown in Fig. 4a and b, respectively. The ROC curve, depicted by the blue line, illustrates the performance of the classifier across different thresholds by plotting sensitivity (true positive rate) against 1-specificity (false positive rate).

The LR classifier evidenced an overall accuracy of 0.976 ± 0.016. The AUC scores indicate excellent class discrimination (Class 0: 1.000 ± 0.000, Class 1: 0.997 ± 0.002, Class 2: 0.996 ± 0.004). Moreover, it evidenced consistently high macro-averaged scores Precision_macro: 0.982 ± 0.013, Recall_macro: 0.957 ± 0.028, F1_macro: 0.967 ± 0.022), with the remaining errors mainly arising from adulterated samples (Class 2) being occasionally predicted as synthetic (Class 1) and, less frequently, as natural (Class 0). These results indicate that LR is a robust multiclass classifier in this context. Recent advances in deep learning-based spectral analysis [70] highlight how convolutional neural networks can capture nonlinear spectral correlations and subtle variations in features, suggesting a possible future direction for improving model accuracy and generalization. The confusion matrix evidenced high classification accuracy, with strong diagonal dominance, indicating reliable predictions for each class, with errors limited to a small number of samples primarily involving Class 2. Misclassifications are minimal, occurring only in case of adulterated BEO, especially at lower dilution concentration. A concentration-resolved error analysis of the adulterated class (Class 2; $n = 10$ per level, 15–60% *v*/v) revealed that the residual misclassifications observed in the confusion matrix are not uniformly distributed across adulteration levels. In PCA–LR, errors were concentrated primarily at the lowest adulterant fraction (15% v/v), where 7/10 spectra were misclassified (Class 1), and to a lesser extent at 60% v/v (2/10 misclassified as Class 0), while all adulterated samples at 30–55% were correctly recognized as Class 2. This pattern is consistent with borderline samples in the low-dimensional PCA score space, where class overlap becomes more pronounced when adulteration fingerprints are weaker (particularly at low adulterant fractions) and may resemble spectral variability of the non-adulterated classes, leading to ambiguous posterior probabilities and occasional confusion between neighbouring classes. This technique enables the easy identification of adulterated products, helping to limit fraud by providing a rapid and

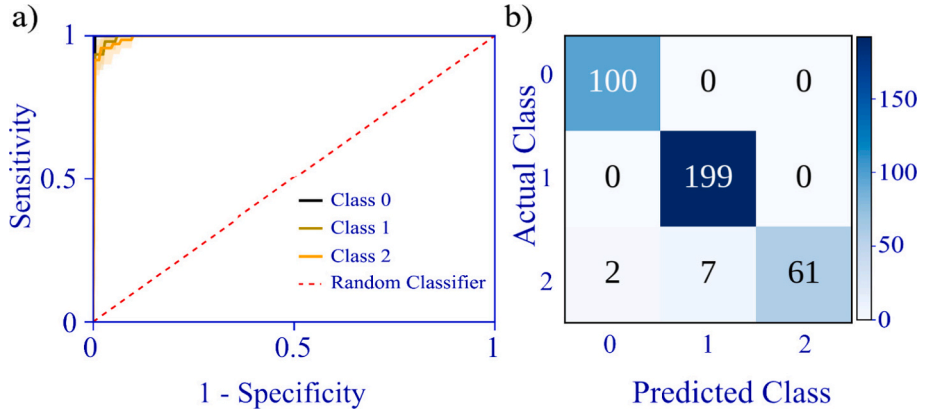

Fig. 4. (a) Receiver operating characteristic ROC curves of LR model (based on 5-fold CV) on the CV set for the overall data set. (b) Confusion matrix averaged over 5-fold CV. Class 0 = Synthetic BEO, Class 1 = Natural BEO, Class 2 = adulterated BEO.

accessible screening tool that can be used by non-specialized personnel.

3.3. NMR validation analysis

A further comparison of the FTIR results were obtained using ^{1}H NMR spectra, as reported in Fig. 5. According to Fig. 5a, the volatile fraction of natural bergamot essential oil in the region between 0.71 and 5.94 ppm is dominated by limonene, β-pinene, linalool, linalyl acetate and γ-terpinene, while the non-volatile fraction in the region between 7 and 8 ppm consists of peaks attributed to bergamottin (5-geranyloxypsoralen), bergapten (5-methoxypsoralen) and citropten (5,7-dimethoxycoumarin) which correspond to the peaks reported in the literature [71–75].

Coumarins which are secondary plant metabolites present in bergamot essential oils have anticancer properties [76]. It has been proven that bergamottin achieves an antiproliferative effect and thus regulates the activity of the SH-SY5Y human neuroblastoma cell line [77]. In addition, furocoumarins can induce phototoxic reactions on the skin after irradiation with ultraviolet A (UVA) or ultraviolet B (UVB) light [76,77], which can be useful in the treatment of skin pigmentation diseases such as vitiligo. Bergamottin, bergapten and citropten share in their structures cyclic α, β-unsaturated fragments with similar multiplicity which indicate the characteristic spectrum of protons in the region between 4.6 and 7.3 ppm. In Table 2 the chemical shifts of recognized natural metabolites are reported.

Several key differences can be observed between the NMR spectra of natural and synthetic bergamot essential oil as evidenced in Fig. 5a and b. The insets of Fig. 5b show process of deconvolution which results in the overlapping peaks that originate from ethanol and 2-(2-hydroxypropoxy)-1-propanol (DPG) [64,78]. The first area of interest is the area between 1.08 and 1.18. ppm in which, due to the complexity of the matrix, overlapping of different peaks occurs. The peaks considered for these two compounds are the multiplicity of H2 proton which resonate at 1.15 ppm from ethanol and multiplicity of H5 and proton which resonate at 1.11 from DPG. Therefore, in this region sharper and less complex peaks are shown, which can be attributed to the synthesized limonene and linalyl acetate. Moreover, the second region of interest is the area between 3.40 and 3.80 ppm which is mainly attributed to DPG. As shown in Table 3, the peak at 3.69 ppm corresponds to H1 proton from both ethanol and DPG, while the peak at 3.72 ppm corresponds to H2 and H4 protons from DPG, and the peak at 3.47 ppm corresponds to H3 proton from DPG.

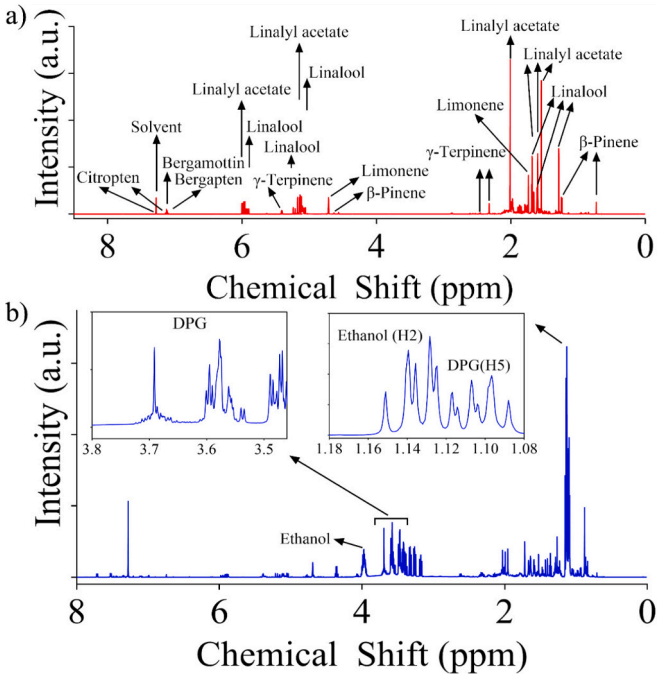

Fig. 5. (a) ^{1}H NMR spectrum of natural BEO and (b) ^{1}H NMR spectrum of synthetic BEO. The insets are related to the specific range from 3.8 to 3.4 ppm and deconvolution between 1.18 and 1.08 ppm.

The third area of interest is the area between 5.00 and 8.00 ppm which is attributed to terpenes. In this area, there are complex, characteristic peaks of terpenoids that indicate the natural origin of the essential oil. As evidenced in Fig. 5 the intensity of the peaks attributed to terpenoids such as linalool, linalyl acetate, γ-terpinene in the synthetic BEO is lower compared to the natural BEO, which can indicate the absence of natural terpenoids in the synthetic BEO.

3.4. Additional remarks

The discriminative spectral regions identified in this study are consistent with alcohol- and ester-containing constituents typically found in synthetic bergamot essential oil formulations. While these features enable effective differentiation between natural, synthetic, and adulterated samples within the investigated dataset, they should not be interpreted as unique markers covering all possible adulteration scenarios, as other adulterants (e.g., foreign essential oils or different carrier oils) may introduce partially overlapping infrared signatures. Alcohol-based carrier solvents are frequently employed in essential-oil adulteration, with DPG and benzyl alcohol among the most commonly reported diluents. These compounds can contribute a broad O—H stretching absorption in the 3600–3100 cm^{-1} region, which has been proposed as an indicator of alcohol-containing adulteration patterns; however, in a quality-control context this signal should be regarded as a classification flag rather than a diluent-specific chemometric identification. In addition, variations around ~1340 cm^{-1} may reflect changes within the fingerprint region associated with synthetic formulations and compositional modifications, including the addition of synthetic compounds (e.g., linalool and linalyl acetate) and/or blending with lower-cost oils. Overall, these spectral cues support the ability of the proposed FTIR-ATR chemometric framework to discriminate authentic natural BEO from adulterated samples in the conditions investigated here. This latter validation further indicates that FTIR along with PCA-LR algorithm can be employed for rapid assessment of BEO authenticity providing reliable results.

4. Conclusions

In this study, FTIR–ATR spectroscopy combined with multivariate chemometric analysis was demonstrated as a rapid and non-destructive approach for the authentication of bergamot essential oil. Clear compositional differences were observed between natural and synthetic bergamot essential oils, particularly related to the presence of alcohol-based components such as ethanol and DPG in synthetic formulations, as well as the absence or reduced contribution of characteristic natural metabolites. The integration of PCA-LR provided robust classification performance within the investigated dataset, while high-resolution NMR spectroscopy served as an independent reference technique supporting the FTIR-based metabolite recognition. These results confirm the suitability of FTIR–ATR spectroscopy as an effective screening tool for the detection of common adulteration practices involving synthetic diluents in high-value essential oils. The integration of PCA–LR provided robust classification performance within the investigated dataset (overall accuracy: 0.976 ± 0.016; macro-averaged AUC: 0.998 ± 0.002; Class 0 AUC: 1.000 ± 0.000; Class 1 AUC: 0.997 ± 0.002; Class 2 AUC: 0.996 ± 0.004), while high-resolution NMR spectroscopy served as an independent reference technique supporting the FTIR-based metabolite recognition. These results confirm the suitability of FTIR–ATR spectroscopy as an effective screening tool for the detection of common adulteration practices involving synthetic diluents in high-value essential oils. Ongoing activities will focus on the development of a dedicated

Table 2
^{1}H and ^{13}C chemical shifts of the recognized metabolites in natural BEO [70–73].

Compound	Group	^{1}H δ (ppm)	^{13}C δ (ppm)
Limonene 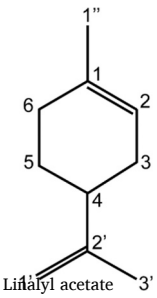	5[a] (CH)	1.43 (m)	27.87 (C5)
	5[b] (CH_2)	1.95 (m)	
	4 (CH)	1.99 (m)	41.05 (C4)
	3[a] (CH_2)	2.03 (m)	30.77 (C3)
	3[b] (CH_2)	1.72 (m)	30.77 (C3)
	1 (—C—)	/	133.72 (C1)
	6[a] (CH_2)	2.05 (m)	30.74 (C6)
	6[b] (CH^2)	2.00 (m)	
	2′ (—C—)	/	150.34 (C2')
	1′ (CH_2)	4.70 (m)	108.33 (C1')
	1″ (CH_3)	1.64 (m)	23.44 (C1")
	3′ (CH_3)	1.72 (s)	20.67(C3')
Linalyl acetate 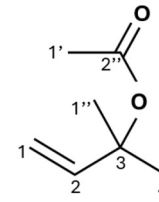	1[a] (CH_2)	5.12 (dm)	111.71(C1)
	1[b] (CH_2)	5.11(dm)	
	2 (CH)	5.93 (dd)	141.78 (C2)
	3 (—C—)	/	82.74 (C3)
	4 (CH_2)	1.58 (m)	39.67 (C4)
	5 (CH_2)	1.99 (m)	22.44 (C5)
	6 (CH)	5.10 (m)	124.31 (C6)
	7 (—C—)	/	123.78 (C7)
	8 (CH3)	1.72 (s)	22.15 (C8)
	1‴ (CH_3)	1.66 (s)	17.76 (C1"')
	1″ (CH_3)	1.52 (s)	25.67 (C1")
	1′ (CH_3)	2.04 (s)	167.19 (C1')
Linalool 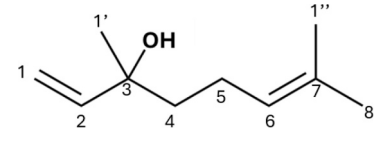	1[a] (CH_2)	5.21 (dm)	111.7 (C1)
	1[b] (CH_2)	5.22 (dm)	
	2 (CH)	5.92 (d)	145.00 (C2)
	3 (—C—)	/	73.28(C3)
	4 (CH_2)	1.43 (m)	42.25 (C4)
	5 (CH_2)	2.03 (m)	25.66 (C5)
	6 (CH)	5.06 (m)	124.45 (C6)
	7 (—C—)	/	133.69 (C7)
	8 (CH_3)	1.67 (s)	22.93 (C8)
	1″ (CH_3)	1.59 (s)	17.77 (C1")
	1′ (CH_3)	1.26 (s)	27.86 (C1')
β-pinene 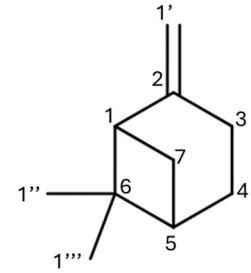	1'[a] (CH_2)	4.67(m)	108.22 (C1)
	1'[b] (CH_2)	4.70 (m)	
	1″ (CH_3)	0.71 (s)	23.44 (C1")
	1‴ (CH_3)	1.22 (s)	23.44 (C1"')
	2 (—C—)	/	150.24 (C2)
	3[a] (CH_2)	2.30 (m)	21.08 (C3)
	7[a] (CH_2)	2.33 (m)	26.02 (C7)
	7[b] (CH_2)	2.60 (m)	
	4[a] (CH_2)	1.64 (m)	23.81 (C4)
	5 (CH)	1.95 (m)	27.04 (C5)
	1 (CH)	1.46 (m)	51.71 (C1)
γ-terpinene 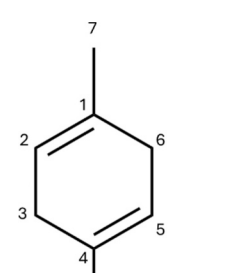	6 (—C—)	/	40.82 (C6)
	1(—C—)	/	131.64
	6(CH_2)	2.46 (m)	27.48-C6
	5(CH)	5.41 (m)	116.08-C5
	4(—C—)	/	141.80
	3(CH_2)	2.46 (m)	30.77-C3
	2(CH)	5.41(m)	116.08-C2
	2'(CH)	2.31(m)	33.81-C2'
	1'(CH_3)	1.02 (d)	21.42-C1'-C3'
	3'(CH_3)		
	7(CH_3)	1.66 (s)	23.53-C7

(*continued on next page*)

Table 2 (*continued*)

Compound	Group	^{1}H δ (ppm)	^{13}C δ (ppm)
Bergamottin	6(CH)	6.01(dm)	113.07-C6
	5(CH)		149.83-C5
	4(CH)		135.06-C4
	3(CH)		112.92-C3
	9(CH)	7.13(s)	145.08-C9
	1'(CH_2)	4.71(m)	73.10-C1'
	2'(CH)		123.46-C2'
	3'(—C—)		144.82-C3'
	6'(CH)		116.08-C6'
	7'(—C—)		131.90-C7'
Bergapten	6(CH)	6.01 (dm)	
	5(CH)		149.83-C5
	9(CH)	7.12 (s)	
	1′ (CH_3)	4.56 (s)	
Citropten	3(CH)	6.00 (dm)	
	4(CH)	7.27 (dm)	135.09-C4

Table 3
^{1}H and ^{13}C chemical shifts of the recognized metabolites in synthetic BEO [64,77].

Compound	Group	^{1}H δ (ppm)	^{13}C δ (ppm)
Ethanol	1 (CH_2)	3.69 (m)	54.19 (C1)
	2 (CH_3)	1.15 (m)	18.64 (C2)
2-(2-hydroxypropoxy)-1-propanol (DPG)	1 (CH_2)	3.69 (m)	65.87 (C1)
	2 (CH)	3.72 (m)	79.27 (C2)
	3 (CH_2)	3.47 (m)	74.98 (C3)
	4 (CH)	3.72(m)	67.10 (C4)
	5(CH_3)	1.11 (m)	18.67 (C5)
	1′ (CH_3)	1.15 (m)	15.72 (C1')

integrated device that leverages the key spectral features identified in this study to enable fast, reliable, and practical screening for safeguarding the quality and authenticity of bergamot essential oil.

Declaration of competing interest

The authors declare that they have no known competing financial interests or personal relationships that could have appeared to influence the work reported in this paper.

Acknowledgments

This research was partially supported by the University of Rijeka, Croatia, project uniri-iskusni-tehnic-23-217. Open access funding provided by Università degli Studi Magna Graecia di Catanzaro within the CRUI-CARE Agreement.

Data availability

Data will be made available on request.

References

[1] S. Ali, R. Ekbbal, S. Salar, S.A. Yasheshwar, S. Ali, A.K. Jaiswal, M. Singh, D. K. Yadav, S. Kumar, Gaurav., Quality standards and pharmacological interventions of natural oils: current scenario and future perspectives, ACS Omega 8 (43) (2023) 39945–39963.
[2] M. Zuzarte, L. Salgueiro, Essential oils chemistry, in: D. de Sousa (Ed.), Bioactive Essential Oils and Cancer, Springer, 2015.
[3] M. Dubnicka, B. Cromwell, M. Levine, Investigation of the adulteration of essential oils by GC-MS, Curr. Anal. Chem. 16 (8) (2020) 965–969.
[4] M. Momtaz, S.Y. Bubli, M.S. Khan, Mechanisms and health aspects of food adulteration: a comprehensive review, Foods 12 (1) (2023) 199.
[5] Y. Zambito, A.M. Piras, A. Fabiano, Bergamot essential oil: a method for introducing it in solid dosage forms, Foods 11 (23) (2022) 3860.
[6] M. Valussi, D. Donelli, F. Firenzuoli, M. Antonelli, Bergamot oil: botany, production, pharmacology, Encyclopedia 1 (2021) 152–176.
[7] F. Gionfriddo, E. Postorino, G. Calabrò, Removal of furocoumarins from bergamot peel oil, Perfumer and Flavorist 29 (2004) 48–53.
[8] Y. Liang, D. Xie, K. Liu, Y. Cao, X. Dai, X. Wang, J. Lu, X. Zhang, X. Li, Bergapten: a review of its pharmacology, pharmacokinetics and toxicity, Phytother. Res. 33 (3) (2019) 700–711.
[9] D. Scuteri, L. Rombolà, M. Crudo, C. Watanabe, H. Mizoguchi, S. Sakurada, K. Hamamura, T. Sakurada, P. Tonin, M.T. Corasaniti, G. Bagetta, Preclinical characterization of antinociceptive effect of bergamot essential oil and of its fractions for rational translation in complementary therapy, Pharmaceutics 14 (2) (2022) 312.
[10] Y. Jiang, T.V. Nguyen, J. Jin, Z.N. Yu, C.H. Song, O.H. Chai, Bergapten ameliorates combined allergic rhinitis and asthma syndrome after PM2.5 exposure by balancing Treg/Th17 expression and suppressing STAT3 and MAPK activation in a mouse model, Biomed. Pharmacother. 164 (2023) 114959.
[11] G.P.P. Kamatou, A.M. Viljoen, Linalool – a review of a biologically active compound of commercial importance, Nat. Prod. Commun. 3 (7) (2008) 1183–1192.
[12] S. Adorisio, I. Muscari, A. Fierabracci, T.T. Thuy, M.C. Marchetti, E. Ayroldi, D. V. Delfino, Biological effects of bergamot and its potential therapeutic use as an

anti-inflammatory, antioxidant, and anticancer agent, Pharm. Biol. 61 (2023) 639–646.
[13] S. Perna, D. Spadaccini, L. Botteri, C. Girometta, A. Riva, P. Allegrini, G. Petrangolini, V. Infantino, M. Rondanelli, Efficacy of bergamot: from anti-inflammatory and anti-oxidative mechanisms to clinical applications as preventive agent for cardiovascular morbidity, skin diseases, and mood alterations, Food Sci. Nutr. 7 (2) (2019) 369–384.
[14] Y. Yang, M. Trevethan, S. Wang, L. Zhao, Beneficial effects of citrus flavanones naringin and naringenin and their food sources on lipid metabolism: an update on bioavailability, pharmacokinetics, and mechanisms, J. Nutr. Biochem. 104 (2022) 108967.
[15] E. Janda, A. Lascala, C. Martino, S. Ragusa, S. Nucera, R. Walker, S. Gratteri, V. Mollace, Molecular mechanisms of lipid- and glucose-lowering activities of bergamot flavonoids, PharmaNutrition 4 (2016) S8–S18.
[16] M.C. Nauman, J.J. Johnson, Clinical application of bergamot (Citrus bergamia) for reducing high cholesterol and cardiovascular disease markers, Integrative Food, Nutrition, and Metabolism 6 (2) (2019) 1–12.
[17] V. Mazzarello, E. Gavini, G. Rassu, M.G. Donadu, D. Usai, G. Piu, V. Pomponi, F. Sucato, S. Zanetti, M.A. Montesu, Clinical assessment of new topical cream containing two essential oils combined with tretinoin in the treatment of acne, Clin. Cosmet. Investig. Dermatol. 13 (2020) 233–239.
[18] N. Wongsukkasem, O. Soynark, M. Suthakitmanus, E. Chongdiloet, C. Chairattanapituk, P. Vattanikitsiri, T. Hongratanaworakit, S. Tadtong, Antiacne-causing bacteria, antioxidant, anti-tyrosinase, anti-elastase and anti-collagenase activities of blend essential oil comprising rose, bergamot, and patchouli oils, Nat. Prod. Commun. 13 (5) (2018) 639–642.
[19] Z. Aumeeruddy-Elalfi, N. Lall, B. Fibrich, A.B. Van Staden, M. Hosenally, M. F. Mahomoodally, Selected essential oils inhibit key physiological enzymes and possess intracellular and extracellular antimelanogenic properties in vitro, J. Food Drug Anal. 26 (1) (2018) 232–243.
[20] J.B. Sharmeen, F.M. Mahomoodally, G. Zengin, F. Maggi, Essential oils as natural sources of fragrance compounds for cosmetics and cosmeceuticals, Molecules 26 (3) (2021) 666.
[21] M. Miastkowska, E. Lasoń, Water-based nanoperfumes, in: A. Nanda, S. Nanda, T. A. Nguyen, S. Rajendran, Y. Slimani (Eds.), Nanocosmetics, Elsevier, 2020, pp. 173–183.
[22] A. Capetti, C. Marengo, E. Cagliero, E. Liberto, C. Bicchi, P. Rubiolo, B. Sgorbini, Adulteration of essential oils: a multitask issue for quality control. Three case studies: *Lavandula angustifolia* mill., *Citrus Limon* (L.) Osbeck, and *Melaleuca alternifolia* (Maiden & Betche) Cheel, Molecules 26 (2021) 5610.
[23] P.S. Vankar, Essential oils and fragrances from natural sources, Resonance 9 (2004) 30–41.
[24] N.S. Aghili, M. Rasekh, H. Karami, O. Edriss, A.D. Wilson, J. Ramos, Aromatic fingerprints: VOC analysis with e-nose and GC-MS for rapid detection of adulteration in sesame oil, Sensors 23 (2023) 6294.
[25] S.K. Bhardwaj, K. Dwivedi, D.D. Agarwal, A review: HPLC method development and validation, International Journal of Analytical and Bioanalytical Chemistry 5 (4) (2015) 76–81.
[26] J.L. Wolfender, HPLC in natural product analysis: the detection issue, Planta Med. 75 (2009) 719–734.
[27] M. Swartz, HPLC detectors: a brief review, J. Liq. Chromatogr. Relat. Technol. 33 (2010) 1130–1150.
[28] S. Tripathi, Decoding analytical excellence: navigating the pros and cons of HPLC technology, International Journal of Pharmaceutical and Healthcare Innovation 1 (2023) 1–6.
[29] A.H.M. Emwas, The strengths and weaknesses of NMR spectroscopy and mass spectrometry with particular focus on metabolomics research, in: J. Bjerrum (Ed.), Metabonomics: Methods in Molecular Biology 1277, Humana Press, 2015, pp. 1–16.
[30] D. Castejón, J. Segura, K.P. Cruz-Díaz, V. Remiro, M.E. Fernández-Valle, M. D. Romero de Ávila, P. Villa, M.A. Cambero, A metabolomics study by 1H HRMAS NMR: from sheep milk to a pressed-curd cheese: a proof of concept, Analytica 5 (2024) 170–186.
[31] E. Lazzari, T. Schena, M.C.A. Marcelo, C.T. Primaz, A. Nunes Silva, M. Flores Ferrao, T.R. Bjerk, E.B. Caramão, Classification of biomass through their pyrolytic bio-oil composition using FTIR and PCA analysis, Ind. Crop. Prod. 111 (2018) 856–864.
[32] B. Liu, Y. Li, L. Zhang, J. Wang, Interpretation of FTIR spectra by principal components–artificial neural networks, Spectroscopy Letters 39 (4) (2006) 373–385.
[33] V. Adiania, S. Gupta, R. Ambolikar, P.S. Variyar, Development of a rapid method to assess microbial quality of minimally processed pomegranate arils using FTIR, Sens. Actuators B 260 (2018) 800–808.
[34] F. Frank, B. Baumgartner, B. Lendl, Metal-organic frameworks combined with mid-infrared spectroscopy for the trace analysis of phosphates in water, Sens. Actuators B 399 (2024) 134778.
[35] A.T. Mogharbel, A. Hameed, A.A. Sayqal, H.A. Katouah, S.D. Al-Qahtani, F.A. Saad, N.M. El-Metwaly, Preparation of carbon dots-embedded fluorescent carboxymethyl cellulose hydrogel for anticounterfeiting applications, Int. J. Biol. Macromol. 238 (2023) 124028.
[36] A. Almahri, A. Albandary, A.M. Al-Bonayan, R.M.S. Attar, A. Karkashan, B. Abbas, S.D. Al-Qahtani, N.M. El-Metwaly, Multifunctional lipophobic polymer dots from cyclodextrin: antimicrobial/anticancer laborers and silver ions chemo-sensor, ACS Omega 8 (19) (2023) 16956–16965.
[37] A.R.Z. Almotairy, O. Alaysuy, S. Ibarhiam, S.O. Alzahrani, N.M. El-Metwaly, Photoluminescent dual-mode anticounterfeiting stamp using self-healable tricarboxy cellulose and polyvinyl alcohol hybrid hydrogel, J. Mol. Liq. 376 (2023) 121495.
[38] A. Almahri, K. Alkhamis, A.F. Qarah, N.M. Alatawi, A. Bayazeed, R.B. Alnoman, N. M. El-Metwaly, Preparation of polyacrylonitrile-based solution blow spinning fluorescent nanofibers from perylene-doped silica nanoparticles, Polymer-Plastics Technology and Materials 62 (18) (2023) 2390–2402.
[39] B. Diehl, Principles in NMR spectroscopy, in: NMR Spectroscopy in Pharmaceutical Analysis 1, Elsevier, 2008, pp. 1–41.
[40] R. Popescu, D. Costinel, O.R. Dinca, A. Marinescu, I. Stefanescu, R.E. Ionete, Discrimination of vegetable oils using NMR spectroscopy and chemometrics, Food Control 48 (2015) 84–90.
[41] M.C. Martínez-Bisbal, N. Carbó Mestre, R. Martínez-Máñez, J. Bauzá, M. Alcañiz Fillol, Microalgae degradation follow-up by voltammetric electronic tongue, impedance spectroscopy, and NMR spectroscopy, Sens. Actuators B 281 (2019) 44–52.
[42] S.A. Kustrin, P. Ristivojevic, V. Gegechkori, T.M. Litvinova, D.W. Morton, Essential oil quality and purity evaluation via FT-IR spectroscopy and pattern recognition techniques, Appl. Sci. 10 (2020) 7294.
[43] S. Kumari, A. Kumari, D.K. Singh, Swift and precise detection of argemone oil adulteration in virgin coconut oil by implementing ATR-FTIR spectroscopy integrated with multivariate chemometrics and regression modelling, Vib. Spectrosc. 126 (2023) 103525.
[44] D.A. Rusak, L.M. Brown, S.D. Martin, Classification of vegetable oils by principal component analysis of FTIR spectra, J. Chem. Educ. 80 (5) (2003) 541.
[45] S.R. Broderick, C. Suh, J. Provine, C.S. Roper, R. Maboudian, R.T. Howe, K. Rajan, Application of principal component analysis to a full profile correlative analysis of FTIR spectra, Surf. Interface Anal. 44 (3) (2012) 365–371.
[46] S.A. Pullano, G. Marcianò, M.G. Bianco, G. Oliva, V. Rania, C. Vocca, E. Cione, G. De Sarro, L. Gallelli, P. Romeo, A. La Gatta, A.S. Fiorillo, FT-IR analysis of structural changes in ketoprofen lysine salt and KiOil caused by a pulsed magnetic field, Bioengineering 9 (2022) 503.
[47] A.N. Lima, E.A. Philot, G.H.G. Trossini, L.P.B. Scott, V.G. Maltarollo, K.M. Honorio, Use of machine learning approaches for novel drug discovery, Expert Opin. Drug Discovery 11 (3) (2016) 225–239.
[48] S. Zheng, X. Xu, G. Chen, J. Zhou, F. Ma, C. Du, Rapid detection of phosphorus in water using silicon attenuated total reflectance infrared spectroscopy coupled with the algorithms of deconvolution and partial least squares regression, Sens. Actuators B 380 (2023) 133372.
[49] K.S. Seshadri, R.N. Jones, The shapes and intensities of infrared absorption bands—a review, Spectrochim. Acta 19 (1963) 1013–1085.
[50] D. Cautela, A. Pastore, G. Ferrari, B. Laratta, N. D'Onofrio, M.L. Balestrieri, L. Servillo, D. Castaldo, Global warming threatens the world production of bergamot essential oil, Industrial Crops & Products 172 (2021) 113986.
[51] G. Oliva, L. Manin, S. Valić, S.K. Islam, A.S. Fiorillo, S.A. Pullano, Zeolite 5A mediated palmitic acid detection in tomato seed oil by photoionization detector, Sens. Actuators B 431 (2025) 137428.
[52] G. Oliva, A.S. Fiorillo, T. Antonić Jelić, S. Valić, S.A. Pullano, Thermal desorption from zeolite layer for VOC detection, Solid State Electron. 210 (2023) 108809.
[53] A. Verzera, G. Lamonica, L. Mondello, A. Trozzi, G. Dugo, The composition of bergamot oil, Perfumery and Flavoring 21 (1996) 19–34.
[54] R.A. Yates, J.D. Caldwell, E.G. Perkins, Diffuse reflectance Fourier transform infrared spectroscopy of triacylglycerol and oleic acid adsorption on synthetic magnesium silicate, J. Am. Oil Chem. Soc. 74 (1997) 289–292.
[55] B. Smith, The infrared spectra of polymers IV: rubbers, Spectroscopy 37 (2022) 8–12.
[56] X. Yang, S. Li, J. Xia, J. Song, K. Huang, M. Li, Renewable myrcene-based UV-curable monomer and its copolymers with acrylated epoxidized soybean oil: design, preparation, and characterization, BioResources 10 (2) (2015) 2130–2142.
[57] A.A. Ismail, F.R. van de Voort, J. Sedman, Chapter 4 Fourier transform infrared spectroscopy: Principles and applications, in: In Techniques and Instrumentation in Analytical Chemistry 18, Elsevier, 1997, pp. 93–139.
[58] R. Medel, M.A. Suhm, Predicting OH stretching fundamental wavenumbers of alcohols for conformational assignment: different correction patterns for density functional and wave-function-based methods, Phys. Chem. Chem. Phys. 23 (2021) 5629–5643.
[59] G. Fei, H. Luija, L. Xian, Vibration spectroscopic technique for species identification based on lipid characteristics, International Journal of Agricultural & Biological Engineering 10 (3) (2017) 255–268.
[60] M. Yahaya, J. Yelwa, S. Abdullahi, J. Umar, M. Babakura, Chemical compositions, FTIR and larvicidal activity of essential oils extracted from aromatic plants, Eur. Sci. J. 15 (2019) 1857–7881.
[61] H. Schulz, M. Baranska, Identification and quantification of valuable plant substances by IR and Raman spectroscopy, Vibrational Spectroscopy 43 (2007) 13–25.
[62] E. Truzzi, C. Durante, D. Bertelli, B. Catellani, S. Pellacani, S. Benvenuti, Rapid classification and recognition method of the species and chemotypes of essential oils by ATR-FTIR spectroscopy coupled with chemometrics, Molecules 27 (17) (2022) 5618.
[63] A. Stepanyuk, A. Kirschning, Synthetic terpenoids in the world of fragrances: Iso E super® is the showcase, Beilstein J. Org. Chem. 15 (2019) 2590–2602.
[64] J. Ottavioli, J. Casanova, A. Bighelli, Identification and quantitative determination of dipropylene glycol in terpene mixtures using 13C NMR spectroscopy, Spectrosc. Lett. 44 (2011) 221–228.
[65] T. Marshall, N.S. Dosoky, P. Satyal, W.N. Setzer, Aroma compounds of carrier oils, Applied Chemistry 3 (2023) 546–580.

[66] V.A. Semikolenov, I.I. Ilyna, I.L. Simakova, Linalool synthesis from α-pinene: kinetic peculiarities of catalytic steps, Appl. Catal. Gen. 211 (1) (2001) 91–107.
[67] R. Nandiyanto, R. Ragadhita, M. Fiandini, I. Ijost, Interpretation of Fourier transform infrared spectra (FTIR): a practical approach in the polymer/plastic thermal decomposition, Indonesian Journal of Science and Technology 8 (2023) 113–126.
[68] N. Cebi, O. Taylan, M. Abusurrah, O. Sagdic, Detection of orange essential oil, isopropyl myristate, and benzyl alcohol in lemon essential oil by FTIR spectroscopy combined with chemometrics, Foods 10 (2021) 27.
[69] A. Martin, V. Silva, L. Perez, J. García-Serna, M.J. Cocero, Direct synthesis of linalyl acetate from linalool in supercritical carbon dioxide: a thermodynamic study, Chem. Eng. Technol. 30 (6) (2007) 726–731.
[70] D. Pratticò, F. Laganà, Infrared thermographic signal analysis of bioactive edible oils using CNNs for quality assessment, Signals 6 (3) (2025) 38.
[71] İ. Toprakçı, F. Balci, N.G. Deniz, S. Ortaboy, M. Torun, S. Şahin, Evaluation of mandarin peel as an alternative source of limonene: identification with GC-MS, FTIR and NMR studies, Food Measurement 18 (2024) 1422–1432.
[72] R.A. Salvino, C. Aroulanda, G. De Filpo, G. Celebre, G. De Luca, Metabolic composition and authenticity evaluation of bergamot essential oil assessed by nuclear magnetic resonance spectroscopy, Analytical Bioanalytical Chemistry 414 (2022) 2297–2313.
[73] Y. Liu, C. Ren, Y. Cao, Y. Wang, W. Duan, L. Xie, C. Sun, X. Li, Characterization and purification of bergamottin from *Citrus grandis* (L.) Osbeck cv. Yongjiazaoxiangyou and its antiproliferative activity and effect on glucose consumption in HepG2 cells, Molecules 22 (2017) 1227.
[74] C. Wang, J. Huang, Z. Zhou, P. Xu, J. Shi, Y. Yang, S. Tong, H. Hu, Coumarins from Jinhua Finger Citron: separation by liquid–liquid chromatography and potential antitumor activity, Molecules 28 (2023) 6917.
[75] S. Adorisio, I. Muscari, A. Fierabracci, T. Thi Thuy, M.C. Marchetti, E. Ayroldi, D. V. Delfino, Biological effects of bergamot and its potential therapeutic use as an anti-inflammatory, antioxidant, and anticancer agent, Pharm. Biol. 61 (1) (2023) 639–646.
[76] A. Maugeri, G.E. Lombardo, L. Musumeci, C. Russo, S. Gangemi, G. Calapai, S. Cirmi, M. Navarra, Bergamottin and 5-geranyloxy-7-methoxycoumarin cooperate in the cytotoxic effect of *Citrus bergamia* (bergamot) essential oil in human neuroblastoma SH-SY5Y cell line, Toxins 13 (2021) 275.
[77] M. Shaaban, M. Nasr, A.A. Tawfik, M. Fadel, O. Sammour, Bergamot oil as an integral component of nanostructured lipid carriers and a photosensitizer for photodynamic treatment of vitiligo: characterization and clinical experimentation, Expert Opin. Drug Deliv. 18 (1) (2020) 139–150.
[78] I.P. Gerothanassis, A. Troganis, V. Exarchou, K. Barbarossou, Nuclear magnetic resonance (NMR) spectroscopy: basic principles and phenomena, and their applications to chemistry, biology and medicine, Chem. Educ. Res. Pract. 3 (2002) 229–252.